NUCLEAR INSTRUMENTS AND METHODS 145 (1977) 81-90 ; © NORTH-HOLLAND PUBLISHING CO.

CHARACTERISTICS OF AN INTENSE NEUTRON SOURCE BASED ON THE d+Be REACTION

M. J. SALTMARSH, C. A. LUDEMANN, C. B. FULMER and R. C. STYLES*

Oak Ridge National Laboratory†, Oak Ridge, Tennessee 37830, U.S.A.

A neutron source designed for fusion-related radiation damage studies has been built based on the d+Be reaction. Using a 40 MeV, 20 μA deuteron beam from the Oak Ridge Isochronous Cyclotron neutron fluxes of $(1-2)\times 10^{12}$ n/cm^2·s are obtained over an area ~ 50 mm^2. The design of the source is described, together with time-of-flight and activation foil measurements of the thick target neutron yields from the ^{9}Be(d, n) reaction for the angular range from 0° to 90°. A dosimetry procedure based on these measurements is presented. In addition time-of-flight measurements of the thick target neutron yields for the Li(d, n) reaction are reported and compared to the ^{9}Be(d, n) results.

1. Introduction

One of the major concerns of the fusion power technology program is the radiation damage to structural materials caused by the neutrons emitted from a D–T plasma[1]). The high energy (~ 14 MeV) component in a fusion reactor first wall neutron spectrum is expected to produce radiation effects different from those encountered in fission reactors due primarily to the higher yield of nuclear transmutation products, particularly helium. Studies of these radiation effects will require the use of neutron sources with suitable spectral characteristics. Until recently most source development work has been concentrated on the use of the D+T reaction, and neutron fluxes up to 10^{12} n/cm^2·s are available at facilities such as the rotating target source reported by Booth and Barshall[2]).

In this paper we describe a d+Be neutron source based on a 40 MeV deuteron beam from the Oak Ridge Isochronous Cyclotron (ORIC) which provides neutron fluxes of up to 2×10^{12} n/cm^2·s. The source has been used for a number of fusion-related irradiations[3,4]) and has proved to be reliable and easy to operate. Absolute measurements of the neutron yield and energy spectrum from the d+Be reaction were made, and the results used in the development of dosimetry techniques suited to this type of source.

While sources of this type can provide reasonable intensities by today's standards, future materials studies will require far more powerful devices. Efforts are now being made to develop such sources based on both the D+T reaction[5,6]) and the d+Li reaction[7–10]). Because of ORNL's interest in d+Li sources, we have also measured the neutron yields from this reaction and have found them to be very similar to those from the d+Be reaction. The dosimetry techniques described in this work should therefore be applicable to the proposed d+Li sources.

2. Source design

A schematic drawing of the beryllium target assembly is shown in fig. 1. The target itself is machined from a cylinder of beryllium 38 mm in diameter and 38 mm long. A 12.7 mm diameter

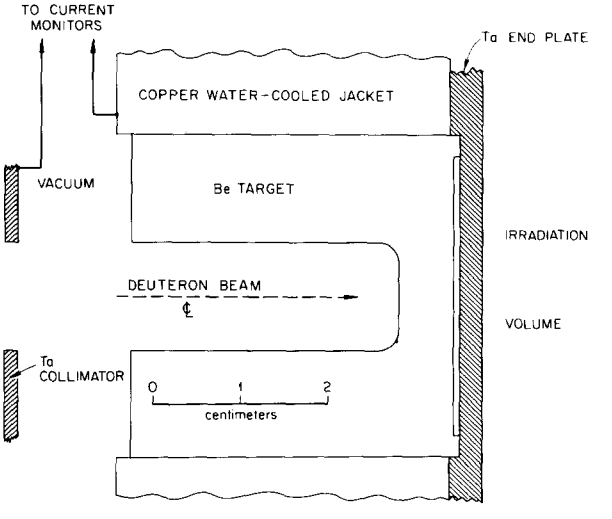

Fig. 1. A schematic of the water-cooled beryllium target. Samples to be irradiated are placed within the irradiation volume immediately downstream of the tantalum end-plate.

* Oak Ridge Associated Universities Undergraduate Research Trainee from Berry College; present address: University of Georgia, Athens, Georgia, U.S.A.

† Work supported by Union Carbide Corporation under contract with the U.S.E.R.D.A.

hole is bored along the axis of the cylinder to within 6.3 mm of the end, thereby leaving just enough material to stop the 40 MeV deuteron beam. The beryllium is surrounded by a copper water-cooled jacket, and springloaded against a tantalum plate which forms the end-window of the cyclotron beam-pipe vacuum system. The tantalum plate is thick enough (2.3 mm) to stop any protons from the ^{9}Be(d, p) reaction.

A quadrupole doublet placed approximately 70 cm upstream of the target, focusses the beam through a 12.7 mm diameter tantalum collimator and onto the target itself. The quadrupole current is set to produce a focus at the position of the sample to be irradiated rather than at the target, a procedure which produces the maximum neutron flux on the sample. At the maximum beam level, which is limited to 20 μA due to activation of the cyclotron extraction system, the beam lost to the tantalum collimator is $\lesssim$ 30 nA, and the diameter of the beam spot at the target is $\lesssim$ 5 mm.

Fig. 2 shows the entire source assembly mounted on a sliding table (1) which permits movement along the beam axis. The sliding seal which connects to the cyclotron beam pipe is at the left (2); a remotely operated target ladder (5) permits insertion of a viewing phosphor at the position of the tantalum collimator. The Be target, copper jacket and tantalum end-plate are all mounted on a stainless steel flange (3) to which the cooling water lines are attached. Also shown is a removable high vacuum chamber (4) which was used to hold samples in a neutron sputtering measurement[3]).

The procedure in setting up for an experiment is to insert the phosphor in place of the tantalum collimator and slide the whole source assembly along the beam direction until the phosphor is located at the position of the sample to be irradiated. Using a low beam intensity ($\sim$ 1 nA) the beam optics are adjusted to provide the smallest possible beam spot on the phosphor and the source assembly is then returned to its normal position. The phosphor is replaced by the tantalum collimator and the beam intensity increased to 20 μA. At this higher beam level the increased load on the cyclotron extraction system results in small changes of the beam trajectory from the cyclotron. Steering magnets are therefore used to re-center the beam by minimizing the beam lost to the collimator.

An irradiation typically lasts 8–36 h with slow beam intensity variations $\lesssim$ 10% occurring during the irradiation period. In addition some interruptions of the beam occur, most being due to sparks in the cyclotron rf and extraction systems resulting in loss of beam for periods of seconds with a frequency varying between $\sim$0.1/h to $\sim$1/h. Calculations indicate that the thermal expansion of the beryllium due to beam heating is sufficient to cause plastic deformation of the target near the interaction region, so these beam interruptions will eventually result in mechanical failure of the target. However, after a total of approximately 300 h of bombardment with an estimated 10^2 beam interruptions no observable damage has occurred except on one occasion when the cooling water was inadvertently valved off. The maximum beam which the target can withstand before melting is not known. In an early run the beam current was increased to 25 μA for a short time ($\sim$4 min) to ensure that some margin of safety existed at the normal operating level. Again no observable damage occurred.

3. Neutron yields from the d+Be reaction

During an irradiation the total beam on the target is monitored to provide an indication of the neutron flux on the irradiated sample. However, beam integration does not provide an adequate measure of fluence at a given point on a sample.

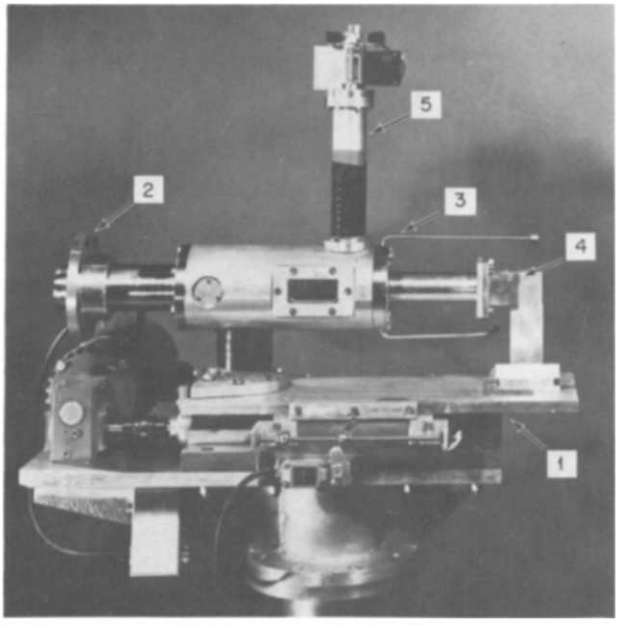

Fig. 2. A photograph of the whole target assembly. The numbers are referred to in the text.

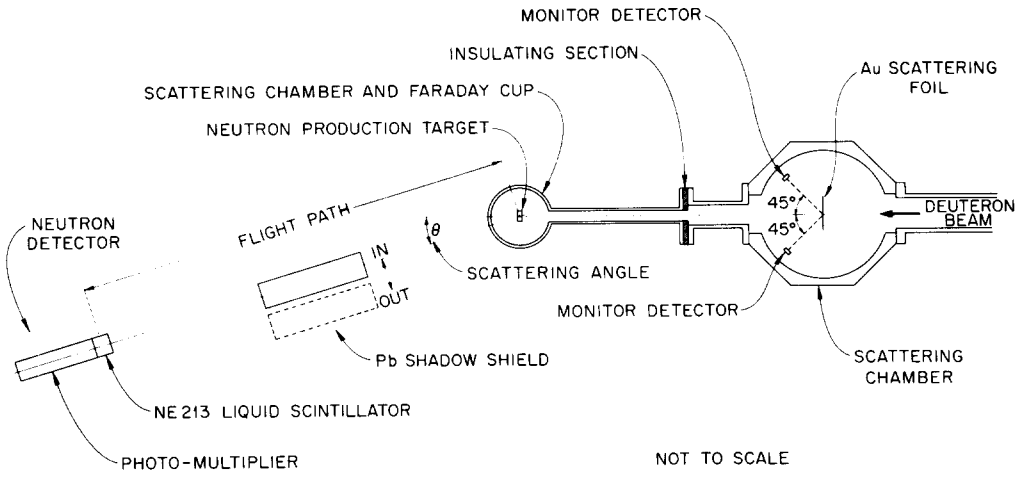

Fig. 3. The layout of the time-of-flight apparatus.

The samples are generally very close (a few mm) to the beryllium target and the geometry is poorly defined. Furthermore, the spatial variation in neutron flux is quite rapid. At a distance of 5 mm from the tantalum end-plate the measured neutron intensity profile is roughly gaussian in shape, with a full width at half maximum ~8 mm. We, therefore, use cobalt and nickel activation foils placed near the sample position to obtain the required dosimetry information, including the spatial variation of the neutron intensity and energy spectrum. The neutron yield measurements used to calibrate these activation foils are described below.

3.1. Time-of-flight measurements

The time-of-flight (TOF) measurements were made using a 40.1 MeV deuteron beam from the ORIC. This beam is pulsed at the cyclotron orbital frequency of 12.97 MHz, providing 2 ns wide pulses every 77.01 ns. With the maximum available flight-path of 3 m the resultant energy resolution varied from ~4% at a neutron energy of 5 MeV to ~15% at 40 MeV. However, neutron energies below 5 MeV could not be reliably measured with this flight path because of overlapping events from successive beam bursts. Accordingly most of the measurements were repeated using a flight path of 0.75 m, which allowed the data to be extended down to $E_n \sim 2$ MeV.

The experimental arrangement is shown in fig. 3. The deuteron beam passed through a thin (7.5 mg/cm^2) gold scattering foil, used in monitoring the beam, and onto the thick (6.3 mm) beryllium target. Neutrons and gamma-rays emitted at an angle θ were detected in a cylindrical cell of NE213 liquid scintillator[11]) 37.3 mm in diameter by 34.1 mm long viewed by a 56AVP photomultiplier tube. The fast timing signal from the photomultiplier tube was used to start a time-to-amplitude converter, the stop signal being derived from every second cycle of the cyclotron rf. A neutron-

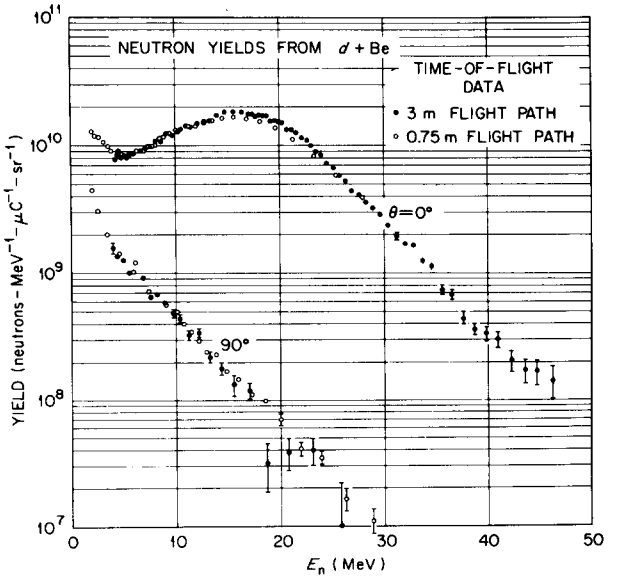

Fig. 4. Time-of-flight data from 40 MeV deuterons on a thick Be target, showing representative error bars. The 0.75 m data (open circles) have been normalized to the 3 m data in the energy ranges 7.5 MeV $< E_n <$ 12.5 MeV. The system resolution (3 m data) varies from ≈200 keV at $E_n = 5$ MeV to ≈6 MeV at $E_n = 40$ MeV.

gamma discrimination circuit was used to route an event into one of two 400-channel time-of-flight spectra. Background events, for example neutrons scattered from the experimental room floor or walls, were measured by placing a 20 cm thick lead shadow shield mid-way between the target and the detector. When the lead shield was removed it was displaced by the smallest possible distance (6 cm), so that the effect of in-scattering from the lead was similar for both foreground and background runs.

The beam current required for these measurements was small, $\lesssim 0.1$ nA. The beam was monitored by counting deuterons scattered at $\pm 45°$ from the thin gold foil. Two detectors were used to eliminate errors due to movements of the beam spot on the gold foil. This secondary monitor was calibrated at intervals during the experiment by increasing the beam current and using the second scattering chamber as a Faraday cup.

The neutron detector threshold was set relative to the half-height of the Compton edge from a ^{22}Na source. Following the definitions of Verbinski et al.[12]) this corresponds to 0.89 light units (LU). For the 3 m runs the threshold was set to be 1.00 LU ($E_n \sim 3.5$ MeV), while for the 0.75 m data a setting of 0.266 LU ($E_n \sim 1.3$ MeV) was used. The detector efficiency at each threshold was calculated for a number of neutron energies in the range 1–50 MeV, using the Monte Carlo code O5S[13]).

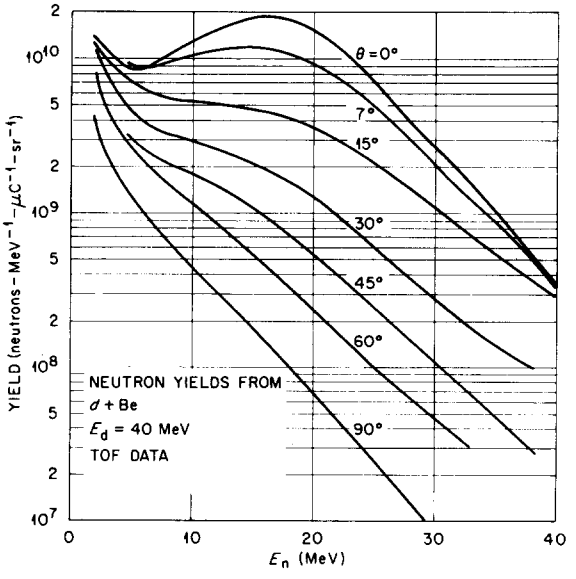

Fig. 5. Time-of-flight data obtained by drawing smooth curves through the results typified by those in fig. 4.

For data analysis the positions of the two gamma-peaks in the appropriate spectrum were obtained by fitting a gaussian peak to the data. The time calibration was obtained from these peak locations by assuming a linear dependence of time-of-flight versus channel number. The neutron spectrum was then converted to an energy spectrum, defining the flight path to be the distance from the geometrical center of the target to the geometrical center of the liquid scintillator. Allowance was made for neutron absorption in the aluminum walls of the scattering chamber (~ 3 mm thick) and the scintillator cell (~ 1.5 mm thick) as well as the air along the flight path. The measured energy spectra from d+Be at 0° and 90° are shown in fig. 4, with the error bars showing statistical uncertainties only. The data from d+Be at all angles studied are shown as smooth curves in fig. 5. The curves for 7° and 45° do not extend below 5 MeV as no runs were made at these angles with a 0.75 m flight path. Monitor uncertainties for the 0.75 m data were typically 8–15% as against 3–4% for the 3 m data. Accordingly, the relative normalization for the two data sets was derived from the total neutron yields for $7.5 \text{ MeV} < E_n < 12.5$ MeV, and the overall normalization defined by the monitor counts for the 3 m data.

The experimental uncertainties for these data come from three sources. First, there are the statistical uncertainties indicated by the error bars in fig. 4. These are generally small. Second, there is a beam monitor uncertainty at each angle, which amounts to approximately 4% at all angles, except for 45° where it is 6%. Finally, and most important, there are uncertainties due to the errors in the efficiency calculations. The resultant overall normalization uncertainty is estimated to be ±15%. Errors in the measured shape of the energy spectrum due to errors in the shape of the efficiency curve are difficult to assess, but are probably less than 10%.

3.2. Foil activation measurements

The neutron yields from the d+Be reaction at $E_d = 39.9$ MeV were measured using the high intensity source described in section 2. Rectangular foils, 50 mm × 120 mm, were mounted on a support in the shape of a circular arc 76.2 mm in radius, and the whole assembly located with the center of the arc at the center of the d+Be interaction region, as shown schematically in fig. 6. Af-

ter exposure for 4 h at a deuteron beam level of 20 μA the foils were removed, allowed to cool for several days, and 6.3 mm diameter discs were punched from them in the pattern indicated fig. 6. The discs were weighed and the gamma activities listed in table 1 were measured using a Ge(Li) detector whose efficiency was calibrated using a standard source.

To convert the measured activities to neutron yields the spectrum-averaged cross sections for the three reactions were computed as a function of scattering angle by folding the spectrum shapes as measured in the time-of-flight runs with the excitation functions shown in fig. 7. For energies

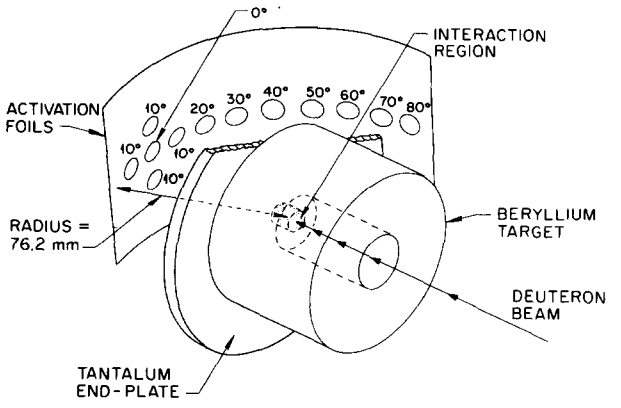

Fig. 6. The experimental arrangement used for the activation measurements in a well-defined geometry. The dimensions of the interaction region were length 6 mm, diameter <5 mm.

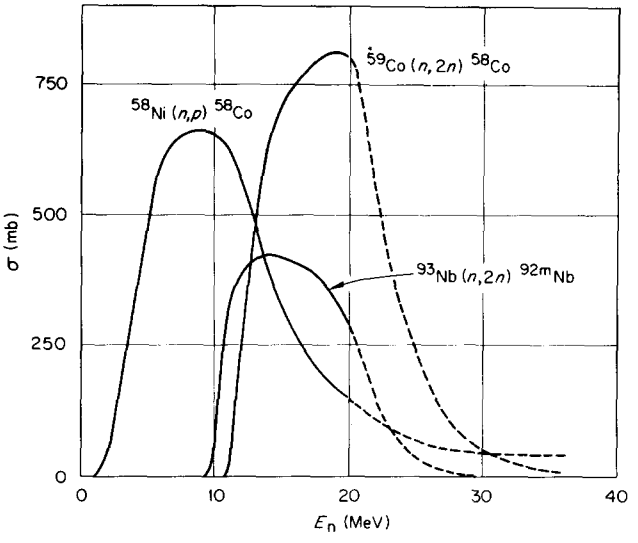

Fig. 7. Excitation functions used to calculate spectrum averaged cross sections. The solid lines represent the energy regions for which data[14–16]) were available; the dotted portions were extrapolations derived from ref. 17.

TABLE 1

Reactions used for activation measurements.

Foil	Reaction	Q-value (MeV)	$\tau_{1/2}$ (d)	E_γ (keV)
Ni (nat)[a]	^{58}Ni(n, p)^{58}Co	0.39	71.3	810.5
Co	^{59}Co(n, 2n)^{58}Co	−10.47	71.3	810.5
Nb	^{93}Nb(n, 2n)^{92m}Nb	− 8.95	10.16	934

[a] Contributions to the ^{58}Co yield from reactions in other nickel isotopes such as ^{60}Ni(n, t) were assumed to be negligible.

$\lesssim$ 20 MeV the available data[14,15]) for the ^{59}Co(n, 2n) and ^{93}Nb(n, 2n) reactions appear to be in reasonably good agreement, but considerable scatter of the experimental results is apparent for the ^{58}Ni(n, p) case[16]). Above 20 MeV there are no data, so the excitation functions were extrapolated using the shapes calculated with the code THRESH[17]). The overall uncertainties in the calculated spectrum averaged cross-sections were estimated to be ±10% for the ^{59}Co(n, 2n) and ^{93}Nb(n, 2n) reactions, and ±15% for the ^{58}Ni(n, p) reaction. In fig. 8 we show the experimental values of neutron yield ($E_n > 2$ MeV) versus angle obtained from the three activation foils, corrected for absorption in the tantalum end-plate. The time-of-flight data are also shown. The errors bars indicate statistical uncertainties only. The solid line represents the mean of the TOF and activation results. The four sets of data are displaced from this curve by an average of −10% (TOF), +10% [^{59}Co(n, 2n)], +1% [^{93}Nb(n, 2n)] and −15%

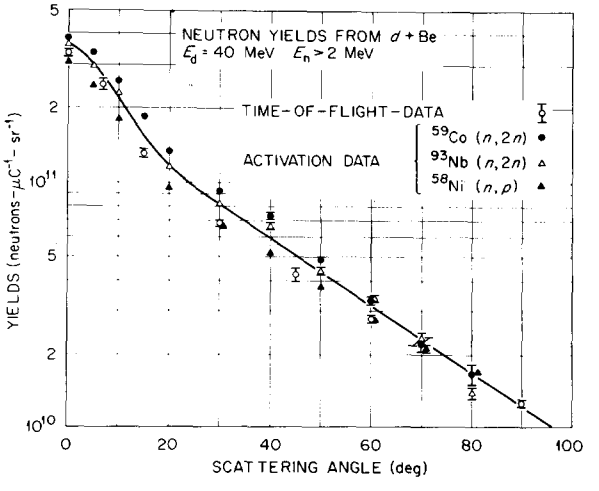

Fig. 8. Experimental values of neutron yield obtained in the present work for 40 MeV deuterons on thick beryllium targets.

TABLE 2
Summary of uncertainties in total neutron yield data.

Data source	Source of uncertainty	Magnitude	Comments
TOF	Counting statistics	Small	Indicated in fig. 4
	Monitor statistics	4–6%	Indicated in fig. 8
	Monitor calibration	3%	
	Detector efficiency	15% (estimated)	Considerable correlation between different angles
^{58}Ni(n, p)	Counting statistics	1–5%	Indicated in fig. 8
	Ge(Li) detector efficiency	5%	Same for all activation data
	Cross sections TOF Spectral shapes	15% (estimated)	Considerable correlation between angles
^{59}Co(n, 2n)	Counting statistics	1–8%	As for ^{58}Ni(n, p)
	Detector efficiency	5%	
	Cross-sections TOF spectral shapes	10% (estimated)	
^{93}Nb(n, 2n)	Counting statistics	1–8%	As for ^{58}Ni(n, p)
	Detector efficiency	5%	
	Cross-sections TOF spectral shapes	10% (estimated)	

TABLE 3
Thick target neutron yields ($E_n > 2$ MeV) from d + Be, $E_d = 40$ MeV. Units are 10^{10} neutrons/μC·sr.

Scattering angle (degrees)	Neutron yields				Average[a]
	TOF data	Activation data			
		^{59}Co(n, 2n)	^{58}Ni(n, p)	^{93}Nb(2, 2n)	
0	33.6 ±1.3	38.7 ±0.4	30.9 ±0.3	35.7 ±0.4	36.0 ±1.8
5		33.7 ±0.4	24.8 ±0.3	29.9 ±0.3	30.0 ±1.5
7	25.1 ±1.3				26.6 ±1.3
10		26.0 ±0.2	18.0 ±0.2	23.1 ±0.2	22.2 ±1.1
15	13.2 ±0.5	18.5 ±0.3			15.4 ±0.8
20		13.4 ±0.2	9.51±0.13	11.6 ±0.2	11.7 ±0.6
30	6.8 ±0.2	9.26±0.17	6.59±0.11	8.19±0.2	8.1 ±0.4
40		7.29±0.23	5.12±0.12	6.65±0.2	5.9 ±0.3
45	4.2 ±0.25				5.05±0.25
50		4.86±0.15	3.74±0.06	4.36±0.16	4.30±0.22
60	2.77±0.1	3.30±0.13	2.79± .07	3.34±0.11	3.14±0.16
70		2.21±0.16	2.10± .08	2.31±0.14	2.30±0.12
80		1.66±0.16	1.68± .06	1.39±0.08	1.67±0.08
90	1.26± .04				1.21±0.06
Scale uncertainty	±15%	±10%	±15%	±10%	±7%

[a] Corresponds to solid line in fig. 8.

[^{58}Ni(n, p)], in reasonable agreement with the estimated uncertainties. In table 2 the various sources of uncertainty are summarized for all sets of data.

In table 3 the results of the four separate measurements of neutron yields ($E_n > 2$ MeV) are listed, together with the average values represented by the solid line in fig. 8. Estimating probable errors for these average values from the complex error matrix implied by the information in table 2 is not practicable. The uncertainties were therefore derived from the scatter of the experimental data points themselves, leading to error estimates of ±5% at each angle, and an overall normalization uncertainty of ±7%.

Thick target neutron yields from the d+Be reaction have previously been measured by Schweimer[18]) at $E_d = 40$ MeV and 53.8 MeV, and by Meulders et al.[19]) at $E_d = 16$ MeV, 33 MeV and 50 MeV. Schweimer's measurement of the neutron energy spectrum at 0° extends down to a neutron energy of 11.5 MeV, and the shape is in good agreement with our results, however, his estimate of the overall yield is approximately 35% lower. Meulders' data include energy spectra at a number of angles for neutron energies $E_n > 3$ MeV. No direct comparison with these data is possible due to the differing deuteron energies, but our data follow the same trends as regards spectral shapes, angular distributions and overall yields.

4. Dosimetry for the d+Be neutron source

Both the neutron flux and energy spectrum vary strongly with distance from the beam axis. Thus the dosimetry must provide a measure of both with a spatial resolution ~1 mm. The basis of the method is to assume that the neutron energy spectrum at any point on the sample is adequately represented by the neutron spectrum seen far from the target at some effective scattering angle (θ_{eff}). Then the neutron dose at a given point on the sample can be completely described by two numbers, the total neutron yield for $E_n > 2$ MeV and the spectrum shape parameter θ_{eff}.

The response of the nickel and cobalt foils in terms of these two parameters is obtained from the yield measurements described in the preceding section. From the activation measurements done in a well-defined geometry, the ratio of the cobalt and nickel activities at each scattering angle are obtained, and used to calculate the ratio of the spectrum averaged cross-sections, $\bar{\sigma}(\mathrm{Co})/\bar{\sigma}(\mathrm{Ni})$, as a function of angle. The results are shown in fig. 9. The solid line in fig. 8, which is our best estimate of the total neutron yield, is used in conjunction with the same activation measurements to calculate the values of $\bar{\sigma}(\mathrm{Co})$ and $\bar{\sigma}(\mathrm{Ni})$ as function of scattering angle. These results (a) are given in table 4, together with the values (b) previously estimated from the time-of-flight data and the published cross sections. [Strictly speaking the nickel values include a contribution from competing reactions such as ^{60}Ni(n, t)^{58}Co, however the correction is probably $< 5\%$ and does not affect the present discussion.] The dosimetry procedure which we use is to measure the activity induced on the cobalt and nickel foils at a given location, compute the ratio $\bar{\sigma}(\mathrm{Co})/\bar{\sigma}(\mathrm{Ni})$ and then obtain θ_{eff} from fig. 9. Knowing θ_{eff} the value of $\bar{\sigma}(\mathrm{Co})$[or $\bar{\sigma}(\mathrm{Ni})$] can be obtained from table 4, and the total neutron fluence calculated.

An example of the method is illustrated in fig. 10. The cobalt and nickel foils were in the form of 25 mm diameter discs, approximately 0.05 mm

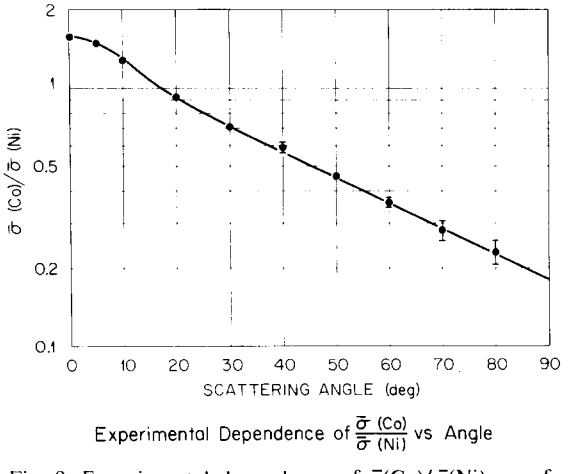

Fig. 9. Experimental dependence of $\bar{\sigma}(\mathrm{Co})/\bar{\sigma}(\mathrm{Ni})$ as a function of angle for neutrons emitted from a thick target bombarded with 40 MeV deuterons.

TABLE 4

Estimates of the spectrum-averaged cross-sections (in mb) for various reactions as a function of scattering angle. Values labeled (a) are used for dosimetry (see text). Values labeled (b) were calculated from time-of-flight data and available cross-section data.

θ (degrees)	^{58}Ni(n, p)^{58}Co $\bar{\sigma}$(Ni)		^{59}Co(n, 2n)^{58}Co $\bar{\sigma}$(Co)		^{93}Nb(n, 2n)^{92m}Nb $\bar{\sigma}$(Nb)	
	(a)[a]	(b)	(a)	(b)	(a)	(b)
0	270	316±47	424	394±39	205	210±20
5	270		400		195	
7	270	330±50	383	332±33	187	183±18
10	272		348		174	
15	278	341±51	300	257±26	149	146±15
20	283		260		131	
30	298	369±55	212	186±19	116	117±12
40	313		175		103	
45	320	386±58	161	168±17	98	113±11
50	329		148		93	
60	343	375±56	124	116±12	83	83±8
70	361		101		74	
80	380		87		66	
90	400	368±55	72	76±8	58	60±6

[a] Includes contributions from competing reactions such as ^{60}Ni(n, t)^{58}Co.

thick, placed perpendicular to the beam axis at a distance of 10 mm from the center of the beryllium target. After an irradiation lasting ~26 h, the pair of foils was removed and allowed to cool for several weeks. Discs 1.5 mm in diameter were then punched from the foils in the radial pattern shown on the insert of the upper part of fig. 10. Each small disc was weighed, and the 810.5 keV γ-activity measured with a Ge(Li) detector. From these data the location of the center of the neutron spot (i.e. the maximum activity) was estimated, and the activity of each disc plotted against its distance r from this center, as shown in fig. 10. There is an implicit assumption in this procedure that the neutron intensity countours are circular, which appears to be well justified by the small scatter of the data points in these plots. From the data in the upper part of fig. 10 the two dose parameters, θ_{eff} and neutron yield were calculated and plotted as a function of r as shown in the lower part of the figure. The neutron spot is seen to have a roughly gaussian profile, with a full width at half maximum of 8.5 mm, and a maximum of $\sim 2 \times 10^{17}$ n/cm^2, corresponding to a average flux $\sim 2.1 \times 10^{12}$ n/cm^2·s during the irradiation.

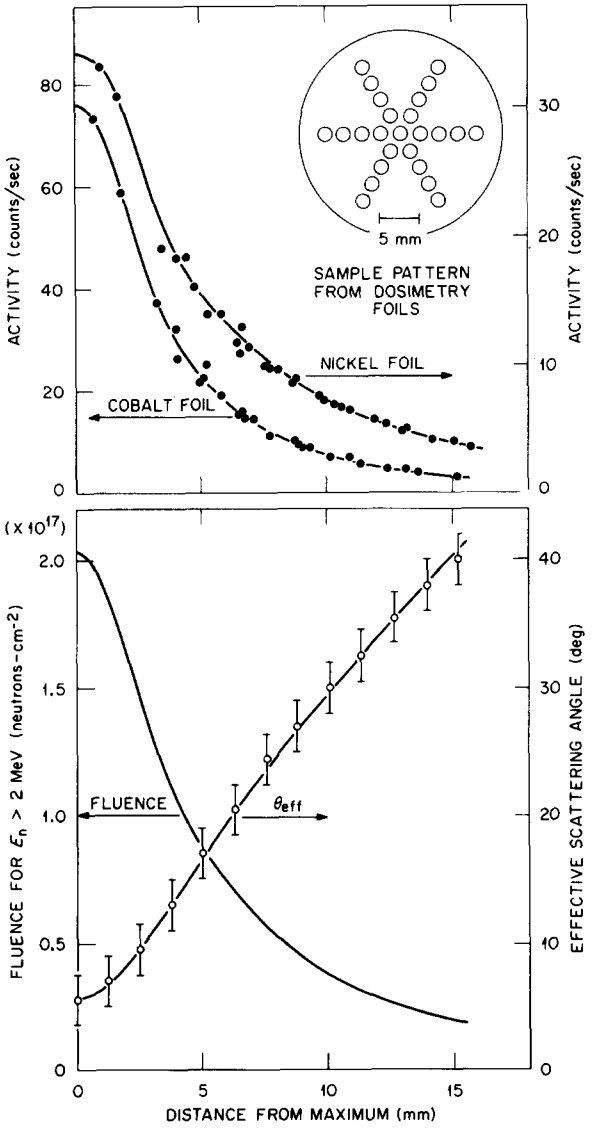

Fig. 10. Dosimetry method used for d+Be neutron source. The upper graphs show the distribution of ^{58}Co activity for the cobalt and nickel dosimetry foils. The lower plots show the spatial dependence of θ_{eff} and neutron yield inferred from these measurements (see section 4).

The overall uncertainty in the the neutron fluence is estimated to be $\pm 10\%$ due largely to the 7% uncertainty of the yield measurements used to calibrate the activation foils. The uncertainty in the definition of spectral shape is difficult to quantify, but in terms of the effective scattering angle it amounts to $\pm 2°$, as indicated in fig. 10.

Although we can give no rigorous justification of this procedure, a plausible argument in support of the basic assumption can be made by noting that neutron energy spectra shown in fig. 5 are composed of two components, a broad peak centered near $E_n = 16$ MeV and an underlying background with a roughly exponential energy dependence. The intensity of the broad peak decreases rapidly with angle while that of the underlying background varies much more slowly. We may express the yield ϕ at an angle θ as

$$\phi(\theta, E) = g_p(\theta)\, f_p(E) + g_b(\theta)\, f_b(E), \qquad (1)$$

where

$f_p(E)$ represents the shape of the broad peak,

$f_b(E)$ represents the shape of the underlying background, and

$g(\theta)$ are the corresponding angular distributions.

When a sample is placed close to the source, so that the beam spot subtends a significant angle at the sample, the spectrum seen by the sample $\Psi(E)$ may be represented by an integral of $\phi(\theta, E)$ over the appropriate angular range, i.e.

$$\psi(E) = \int_{\theta_{min}}^{\theta_{max}} x(\theta)\, \phi(\theta, E)\, d\phi, \qquad (2)$$

where $x(\theta)$ depends upon the beam intensity profile, divergence, etc.

Substituting eq. (1) into eq. (2) we obtain

TABLE 5

Thick target neutron yields ($E_n > 2$ MeV) from d+Li, $E_d = 40$ MeV. Units are 10^{10} neutrons/μC·sr.

Scattering angle (degrees)	Neutron yield TOF data[a]	Renormalized[b]
0	36.7 ±1.8	40.9 ±2.9
7	25.3 ±1.3	38.2 ±2.0
15	11.6 ±0.4	13.0 ±0.9
30	6.28±0.25	6.99±0.50
45	3.73±0.17	4.15±0.30
60	2.48±0.09	2.76±0.19
90	1.43±0.05	1.59±0.11
Scale uncertainty	±15%	±7%

[a] Statistical errors only.
[b] See section 5.

$$\psi(E) = f_p(E) \int_{\theta_{min}}^{\theta_{max}} d\theta\, x(\theta)\, g_p(\theta) + f_b(E) \times$$

$$\times \int_{\theta_{min}}^{\theta_{max}} d\theta\, x(\theta)\, g_b(\theta) = a_p\, f_p(E) + a_b\, f_b(E).$$

This spectrum has the same form as the spectrum $\phi(\theta_{eff}, E)$ at an angle θ_{eff} from a point source, where

$$a_p/a_b = g_p(\theta_{eff})/g_b(\theta_{eff}).$$

Thus, provided that the functions $x(\theta)$, $g_p(\theta)$ and $g_b(\theta)$ are reasonably well behaved, the neutron spectrum seen by a sample placed close to the source can be characterized by the spectrum measured far from the source at some angle θ_{eff}.

Given the assumption represented by eq. (1), i.e. that the spectrum at any angle is the sum of two components whose energy dependence is independent of angle, the above argument is still not rigorous because the finite thickness of the source has been ignored. This effect cannot be evaluated without a knowledge of the thin-target neutron yields for the ^{9}Be(d, n) reaction over the full deuteron energy range of 0–40 MeV.

5. Neutron yields from the d+Li reaction

In the recent ORNL proposal[8]) for an intense neutron generator based on the d+Li reaction, results were reported for the thick target neutron yield from 40 MeV deuteron bombardment of lithium. These data are in disagreement, by a factor of two, with other preliminary results reported in the similar BNL proposal[7]). We have repeated these measurements using the time-of-flight apparatus described previously and the results, shown in fig. 11, are consistent with the earlier

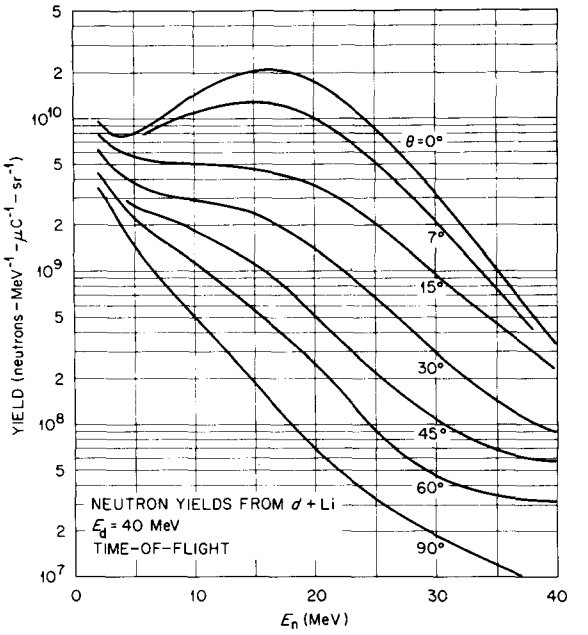

Fig. 11. Neutron yields from 40 MeV deuterons on a thick Li target. The curves were obtained from time-of-flight data in the same manner as those for d+Be (fig. 5).

ORNL data. The total neutron yields for $E_n > 2$ MeV from the present work, which are given in table 5, have sources of error which are similar to those listed in table 2 for the beryllium results. From the beryllium data we see that the time-of-flight results are 10% lower than the average values for the total yields, accordingly the lithium data should be renormalized upwards by this amount, as shown in the final column of table 5. The errors quoted in this column reflect not only statistical errors, but also those due to uncertainties in the shape of the detector efficiency curves.

The results indicate a slightly higher yield for the d+Li reaction as compared to the d+Be reaction as might be expected from the systematics noted by Schweimer[18]). The forward angle spectra also show a reduced contribution at the lower neutron energies. However, the overall similarity of the spectra from the two reactions suggest that d+Be sources will be useful in examining the neutronics of the proposed d+Li sources, and that the dosimetry techniques described here will be applicable to such devices.

Our thanks are due to G. J. Smith for help in the early steps of this work, and to R. P. Cumby for providing the neutron scintillation detector. The

invaluable assistance of M. B. Marshall and the ORIC operating staff is gratefully acknowledged. One of us (RCS) would like to thank Oak Ridge Associated Universities for support as an Undergraduate Research Trainee.

References

[1]) D. Steiner, Nucl. Sci. Engng. **58** (1975) 107; Rev. Mod. Phys. **47**, Suppl. no. 3 (1975).
[2]) R. Booth and H. H. Barshall, Nucl. Instr. and Meth. **99** (1972) 1.
[3]) L. H. Jenkins, T. S. Noggle, R. E. Reed, M. J. Saltmarsh and G. T. Smith, Appl. Phys. Lett. **26** (1975) 426.
[4]) J. B. Roberto, J. Narayan and M. J. Saltmarsh, Proc. Int. Conf. on *Radiation effects and tritium technology for fusion reactors,* Gatlinburg, Tennessee, CONF-750989, vol. 2 (1976) p. 159.
[5]) J. C. Davis, J. D. Anderson, R. Booth, C. M. Logan, and J. E. Osher, Proc. Int. Conf. on *Radiation test facilities for the CTR surface and materials program,* Argonne National Laboratory, ANL/CTR-75-4 (1975) p. 183.
[6]) D. D. Armstrong, C. R. Emigh, K. L. Meier, E. A. Meyer and J. D. Schneider, p. 261 of ref. 5.
[7]) P. Grand (ed.), BNL-20159 (1975).
[8]) M. J. Saltmarsh and R. E. Worsham (eds.), ORNL-TM-5233 (1976).
[9]) CTR materials irradiation testing facility (CMIT) proposal, Hanford Engineering and Development Laboratory (1975).
[10]) Lawrence Livermore Laboratory, LLL-Prop 137 (1976).
[11]) Manufactured by Nuclear Enterprises, Inc., 935 Terminal Way, San Carlos, California 94070, U.S.A.
[12]) V. V. Verbinski, W. R. Burrus, T. A. Love, W. Zobel, N. W. Hill and R. Textor, Nucl. Instr. and Meth. **65** (1968) 8.
[13]) R. E. Textor and V. V. Verbinski, ORNL-4160 (1968).
[14]) ENDF-B-IV, MAT-1199, BNL 17541 (ENDF-201) (1975).
[15]) A. Paulsen and R. Widera, Z. Physik **238** (1970) 23.
[16]) ENDF-B-IV, MAT-1190, BNL 17541 (ENDF-201) (1975).
[17]) S. Pearlstein, J. Nucl. Engng. **27** (1973) 81.
[18]) G. W. Schweimer, Nucl. Phys. **A100** (1967) 537.
[19]) J. P. Meulders, P. Leleux, P. C. Macq and C. Pirart, Phys. Med. Biol. **20** (1975) 235.